Urban Forestry & Urban Greening 88 (2023) 128086

Contents lists available at ScienceDirect

Urban Forestry & Urban Greening

journal homepage: www.elsevier.com/locate/ufug

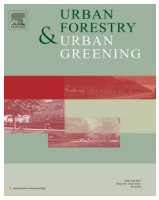

Greening the concrete jungle: Unveiling the co-mitigation of greenspace configuration on $PM_{2.5}$ and land surface temperature with explanatory machine learning

Yan Li [a,b], Yecheng Zhang [b], Qilin Wu [c], Ran Xue [a], Xiaoran Wang [d], Menglin Si [e], Yuyang Zhang [a,*]

[a] Department of Urban Planning and Landscape, North China University of Technology, Beijing 100144, China
[b] School of Architecture, Tsinghua University, Beijing 100084, China
[c] Beijing Tsinghua Tongheng Urban Planning & Design Institute, Beijing 100085, China
[d] School of Architecture and Urban Planning, Beijing University of Civil Engineering and Architecture, Beijing 100044, China
[e] State Key Laboratory of Efficient Utilization of Arid and Semi-arid Arable Land in Northern China, Institute of Agricultural Resources and Regional Planning, Chinese Academy of Agricultural Sciences, Beijing 100081, China

ARTICLE INFO

Handling Editor: Cecil Konijnendijk van den Bosch

Keywords:
Greenspace patch
Urban morphology
Highly-dense urban area

ABSTRACT

In densely populated urban areas, the amount of urban green space (UGS) is limited and increasing it can be challenging due to the high proportion of unvegetated land. Therefore, it is crucial to determine the optimal spatial configuration of UGS to achieve environmental benefits such as reducing $PM_{2.5}$ concentrations and land surface temperature (LST). However, there is limited research on this topic. This study employed an explanatory machine learning method to identify the non-linear relationships between contributing factors and the co-mitigation of $PM_{2.5}$ and LST in highly-dense urban areas, which had three key advantages: improved accuracy, spatially explicit information, and enhanced understanding of complex relationships. The study found that maintaining a UGS proportion of 25–30 % was desirable for mitigating $PM_{2.5}$ and LST. Additionally, maintaining an aggregation index above 97, a patch density above 1650, and a largest UGS patch proportion between 2.00 % and 4.85 % was beneficial for co-mitigation. However, the study found conflicting results between shape complexity and co-mitigation. Surprisingly, higher road density appeared to mitigate both $PM_{2.5}$ and LSTs. Overall, the study highlights the potential of explanatory machine learning methods for sustainable urban environmental management, providing insights into the co-mitigation effects of UGS and urban morphology.

1. Introduction

Global mega-cities are currently facing two parallel challenges, namely heat waves and fine particulate matter ($PM_{2.5}$) air pollution, both of which are manifestations of intensive changes in human settlement patterns, energy use, traffic emissions, industry activities and natural resource pressures caused by rapid urbanization, urban sprawl, and population growth (Imhoff et al., 2010). In highly-dense urban areas, the situation becomes particularly severe due to the limited availability of urban green space (UGS). These limitations can result in both frequent heatwaves and excessively high concentrations of $PM_{2.5}$, exacerbating the environmental challenges faced by these highly-dense urban areas (Han et al., 2015). Exposure to extremely hot weather and high levels of $PM_{2.5}$ concentrations could both result in significant disease burdens and have aroused global attention. Specifically, exposure to high temperatures can cause a notable rise in hospital admissions and mortality rates. Studies have shown that when the daily mean temperature exceeds 28.2 °C, an average temperature rise of 1 °C is associated with an estimated 1.8 % increase in mortality rates (Chan et al., 2012). The senior citizens over 65 years have been elucidated to be more vulnerable to hot weather in highly-dense urban area (Chestnut et al., 1998). Likewise, higher $PM_{2.5}$ exposure is associated with premature death, respiratory disease, lung cancer, cardiovascular disease, and asthma attacks (Kim et al., 2015). In 2019, chronic exposure to $PM_{2.5}$ pollution caused 4.14 million deaths worldwide (95 % uncertainty interval (UI): 3.45–4.80), accounting for 62 % of all deaths due to air

* Corresponding author.
E-mail address: yuyond@ncut.edu.cn (Y. Zhang).

https://doi.org/10.1016/j.ufug.2023.128086
Received 18 April 2023; Received in revised form 13 September 2023; Accepted 14 September 2023
Available online 16 September 2023

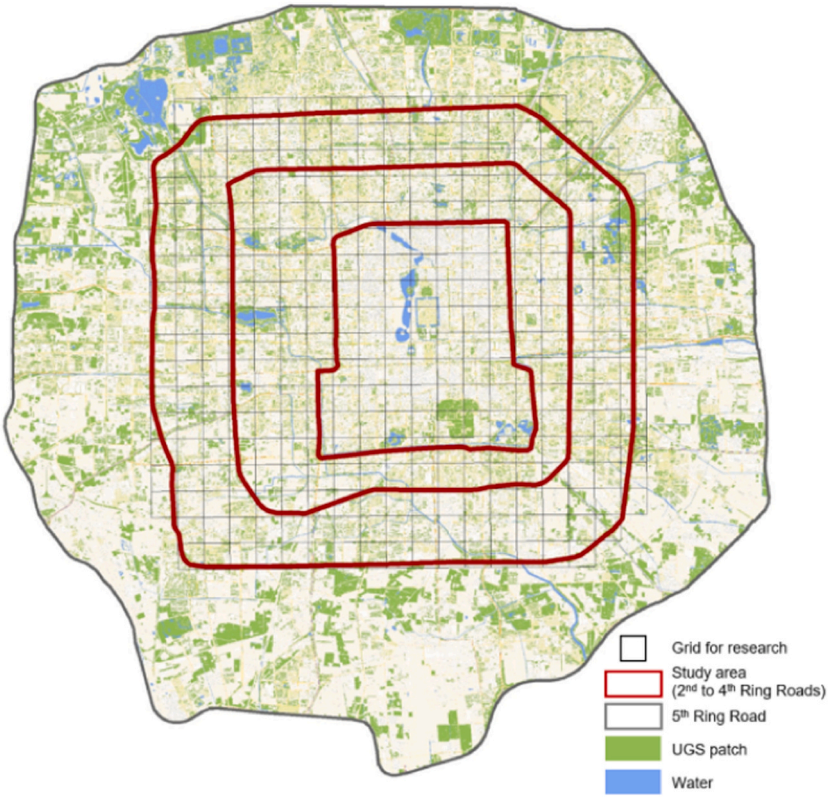

Fig. 1. Study area in Beijing.

pollution.

Several research studies have concentrated on identifying measures to address the adverse impacts of urban heat islands (UHI) or atmospheric $PM_{2.5}$ levels. In general, improving UGS has been widely recognized as a common and efficient strategy address both of these issues (Zhang et al., 2023; Bi et al., 2022a; Yang et al., 2017). The mitigation solutions of UGS for both issues have been specifically explored. In terms of UHI that usually represented by land surface temperature (LST), vegetation can play a role in absorbing solar radiation and converting it to latent heat through evapotranspiration, while trees can offer shade to lower production of sensible heat, resulting in a cooling effect (Lin et al., 2010; Ali-Toudert and Mayer, 2007). For $PM_{2.5}$ concentrations, vegetation could be considered as an air purifier by intercepting atmospheric particulate matter through the secretions of tree leaves, rough foliage, and long fuzz, thereby reducing the concentration of airborne respirable particles (Beckett et al., 2000).

In highly-dense urban areas, the presence of high proportions of unvegetated land surfaces, such as buildings and roads, often results in limited availability and significant difficulties in improving the proportion of UGS (Lo and Jim, 2012). These areas are typically characterized by fragmentation, small size and poor connectivity of UGS (Huang et al., 2017; Zhang et al., 2021). Earlier research has demonstrated that, beyond the proportion of UGS, the spatial configuration can also alleviate the $PM_{2.5}$ concentrations and LST. Therefore, it becomes extremely important to determine the optimal spatial configuration of UGS (Connors et al., 2013), especially for alleviating $PM_{2.5}$ concentrations and LSTs. Regarding $PM_{2.5}$, enhancing the geometric features of vegetation, such as increasing the width of greenbelts, can promote advantageous wind conditions for the deposition of atmospheric PM, leading to an improvement in its interception effect as a physical barrier (Khan and Abbasi, 2001). For example, $PM_{2.5}$ deposition may be undermined by dispersed UGS patches (Zhao et al., 2021). Higher edge complexity of large UGS patches could enhance the deposition ability of UGS by promoting edge effects (Bi et al., 2022b; McDonald et al., 2007). In terms of LST, the seasonal variation is influenced by the topography of the land surface and the diversity of urban green spaces (UGS) (Peng et al., 2018). It was found that the cold island effects were relatively stronger in UGS patches with regular shapes, high connectivity and aggregated distribution (Lin et al., 2020). However, few observational studies have revealed whether these spatial configurations have co-mitigation or conflicting effects on these two hazardous environmental issues. There are two main reasons for this: firstly, there is an interaction between LST and $PM_{2.5}$ in the same season, which can vary greatly geographically even within a city (Huang and Lu, 2018); secondly, among the commonly used remote sensing data that depict UGS, the boundaries of UGS patches fluctuate seasonally due to variations in leaf biomass and/or the leaf area index, rendering direct comparisons between seasons unfeasible. To address these issues, this study focuses on the most severe seasons for PM and LST, exploring whether UGS configuration can effectively address both high summer LST and winter PM issues; the study also introduces Tianditu, which is the official online map of China and provides detailed description of each UGS patch and the edges of UGS patches remain consistent in all seasons.

In the field of geography, spatial statistical models, including Spatial Lag Model (SLM), Spatial Error Model (SEM), Geographical Weighted Regression (GWR) and Multiple Geographical Weighted Regression (MGWR), were commonly employed to estimate the relationships. These models have advantages in estimating local interpretation of features and of a rigorous explanatory framework, which is considered a huge benefit over machine learning regression models. However, the models were limited in their ability to capture non-linear relationships between the explanatory variables and the output, while the cooling effect of UGS and urban heat island mitigation have been extensively argued to be non-linear relationship (Yu et al., 2020). Recently, explainable machine learning has emerged as a proper alternative to statistical models in many fields, particularly in spatial contexts where local interpretation is indispensable as the data are georeferenced. Therefore, in this study, an XGBoost machine learning model was employed, and its results were

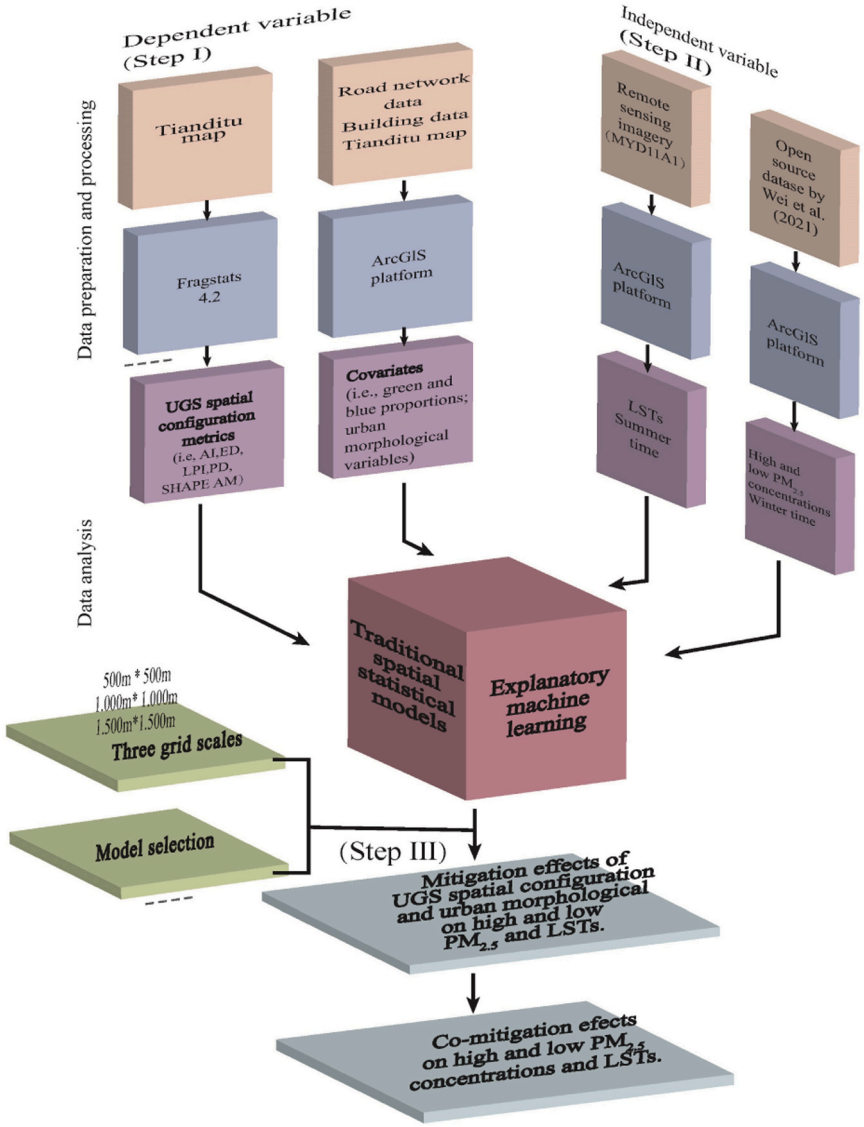

Fig. 2. Methodology framework.

explained using Shapley Additive Explanations (SHAP),to explore the non-linear connections among $PM_{2.5}$, LST and a set of explanatory variables, which has been confirmed to be effective in previous geographical studies (Zhang et al., 2023; Li, 2022).

To summarize, this study seeks to examine the influence of UGS on $PM_{2.5}$ levels and LST, addressing the following research questions: (1) Does the spatial configuration of UGS have a consistent mitigating effect on both? (2) Which configuration factors (e.g., density, aggregation, shape) have positive or negative effects on the mitigation? (3) Is explainable machine learning model the optimal model for the study?

2. Study area and data

2.1. Study area

Regarding the definition of highly-dense urban area, high building density and population density are the main evaluation criteria. The highly-dense area of Beijing, which is within the 4th Ring Road, is considered as the study area (Fig. 1).

The impervious surface area in the study area is approximately 85 % while the area identified as UGS in this study is only 15 %. The high volume of urban traffic significantly contributes to severe heat and air pollution, which represents a grave peril to the health of residents and the prospects of sustainable urban growth. In recent years, Beijing has encountered frequent hot weather during summers, with the mean temperature difference between urban and rural regions exceeding 2 °C (Huang and Lu, 2018; Peng et al., 2016). Meanwhile, the recurrent occurrences of haze and elevated levels of pollutants in this city have garnered global attention. Therefore, there is an urgent need for Beijing to investigate appropriate spatial configurations of UGS to simultaneously mitigate these two harmful issues.

2.2. Data

The LST data utilized in this study was acquired from the Moderate Resolution Imaging Spectroradiometer (MODIS) remote sensing observation data, which were accessed from the National Aeronautics and Space Administration (https://search.earthdata.nasa.gov, accessed on March 9, 2023). The resolution of the data was 1 km × 1 km, and it covered the period from Jun 1 to Aug 31 in 2019 and 2020. The PM2.5 data was derived from satellite images and was available as gridded data with a spatial resolution of 0.01° (roughly 1 km in China) for January 2020 (Wei et al., 2021). The UGS and water bodies were extracted from the map tiles of Tianditu, the initial web mapping service sponsored by

the Chinese government, which can be downloaded from the Shuijingzhu mapping software. The map tiles used in this study was at level 19, with a scale of 1:2256 and a spatial resolution of 0.60 m. Each extracted UGS patch depicted well-defined boundaries of the vegetated land surface across the study area (Zhang et al., 2021). UGS patches situated deep within blocks and communities were frequently disregarded and oversimplified in other commercial maps or remote sensing analyses, but in this study, they were very clearly delineated, which supported accurate calculation of UGS spatial configuration variables and were beneficial for conducting more specific UGS construction guidelines. The data used to analyze urban morphology including building vector data with basic shape and height information, as well as road network data, which were acquired form Amap, a leading navigation company in China.

3. Methodology

In this study, grid-based calculations were performed for its capability of integrating data from various sources and enabling comprehensive analysis across the entire study area. Scale effects were investigated at three different scales, specifically 500 m (1279 grids), 1000 m (385 grids) and 1500 m (152 grids), to validate the consistency of the conclusions and explore potential variations across different scales. These chosen scales encompass a range of spatial extents, ranging from the size of a small community to that of a larger block.

This study consisted of three steps (Fig. 2). The first step was to calculate $PM_{2.5}$ concentrations and LSTs, resulting in three dependent variables, high and low levels of $PM_{2.5}$ and LST. The second step was to calculate spatial configuration variables of UGS, as well as other urban explanatory variables, including water proportion, road density, two-dimensional (2D) and three-dimensional (3D) building form variables, resulting in a total of 14 independent variables. In the final step, assuming that both high and low levels of $PM_{2.5}$ and LSTs concentrations in a grid were correlated with UGS variables, urban morphological variables, as well as LSTs and $PM_{2.5}$ concentrations in adjacent grids, a series of spatial statistical analyses and machine learning spatial regression model were conducted to compare and explore the effects of UGS spatial configuration on $PM_{2.5}$ concentrations and LSTs, and to determine the most appropriate approach based on the validation accuracy results.

3.1. Estimation of LSTs and $PM_{2.5}$ concentrations

The daily instantaneous LSTs product MYD11A1 (~1 km spatial resolution) obtained from Aqua (transit at ~13:30 pm, local solar time) were filtered with LST error less than 2 K (Wan, 2014; Si et al., 2022) and averaged from Jun 1 to Aug 31, in 2019 and 2020, respectively, to represent the maximum LSTs in summer.

The $PM_{2.5}$ concentrations in January 2020 were extracted from Wei et al (Wei et al., 2021)., which can capture $PM_{2.5}$ concentration variations at different spatio-temporal scales with high accuracy, as demonstrated by its high cross-validation R^2 values of 0.86–0.90 and strong predictive ability ($R^2 = 0.80$–0.82) compared to previous studies. Due to the large daily variability of $PM_{2.5}$ concentrations, using monthly averages for each grid may lead to the higher levels dominating the lower ones. The WHO air quality guideline recommends a 24-hour mean of 25 μg/m^3 for $PM_{2.5}$, which can be regarded as the threshold for low-level pollution (Organization, 2006). In contrast, the breakpoint of $>$ 50 μg/m^3 corresponds to the "unhealthy for sensitive populations" category on the Air Quality Index. This value is considered the threshold for high-level pollution (EPA, 2012). Therefore, this study considered 25 ug/m^3 and 50 ug/m^3 as threshold values, and dates with the minimum value greater than 25 and the maximum value less than 50 were considered as low $PM_{2.5}$ concentration levels (low $PM_{2.5}$); while dates with the minimum value greater than 50 were considered as high $PM_{2.5}$ concentration levels (high $PM_{2.5}$).

Table 1
Statistical descriptions of variables.

Types	Variables	Unit	500 m scale				1000 m scale				1500 m scale			
			Min	Max	Mean	Std. D	Min	Max	Mean	Std. D	Min	Max	Mean	Std. D
Area-edge metrics	PD	Patches per 100 ha	16.28	11345.83	1859.40	1486.64	255.41	6496.39	1839.92	1019.64	313.81	3867.17	1841.42	774.75
	ED	Meters per hectare	3.92	1210.29	392.54	168.96	54.45	820.58	387.79	125.33	115.29	692.95	383.98	106.37
	LPI	%	0.03	77.31	2.81	4.58	0.05	58.96	1.73	3.87	0.08	39.52	1.36	3.35
Shape metric	SHAPE_AM	-	1.24	4.734	2.08	0.40	1.30	3.88	2.16	0.31	1.59	3.05	2.20	0.26
Aggregation metric	AI	%	44.99	99.71	95.06	3.09	87.10	99.55	95.58	1.68	92.43	99.40	95.85	1.33
Green and water proportion	PLAND	%	0.06	82.63	15.08	11.13	0.99	69.97	15.35	9.25	3.19	50.88	15.63	7.70
	Water	%	0.00	65.20	2.28	5.88	0.01	29.25	2.30	4.08	0.03	28.17	2.44	4.06
Urban form	den_build	m^2/m^2	0.00	0.88	0.28	0.11	0.06	0.44	0.26	0.07	0.08	0.37	0.25	0.06
	FAR	m^2/m^2	0.00	8.13	1.78	0.91	0.19	4.04	1.63	0.62	0.18	3.11	1.55	0.52
	den_road	m/km^2	0.00	26445.63	5134.96	4366.48	0.00	12837.01	4547.18	2386.59	0	9243.90	4297.56	1719.60

3.2. Estimation of UGS spatial configuration variables and covariates

The selection of spatial configuration variables for UGS is based on four principles, including (1) importance in theoretical understanding and practical application, (2) ease of calculation, (3) interpretability, and (4) minimal redundancy (Connors et al., 2013; Chen et al., 2014; Zhou et al., 2017), and ultimately six variables were included: patch density (PD), edge density (ED), area-weighted mean patch shape (SHAPE_AM), largest patch index (LPI), aggregated index (AI) and UGS proportion (PLAND), all calculated using Fragstats 4.2. Patch Density (PD) is calculated as the number of UGS patches per unit area, reflecting the overall density of patches within the landscape. Edge Density (ED) refers to the total length of UGS patch edges per unit area, indicating the amount of edge habitat within the landscape. Area Weighted Mean Patch Shape (SHAPE_AM) is a measure of the average shape complexity of UGS patches, calculated by considering the proportion of each patch size class in relation to the total UGS area. The Largest Patch Index (LPI) quantifies the proportion of the landscape occupied by the largest UGS patch, providing insights into the dominance and size of the largest UGS feature. The Aggregated Index (AI) serves as a measure of the spatial aggregation or clumping of UGS patches, indicating how closely the UGS patches are distributed within the landscape. Finally, the UGS Proportion (PLAND) denotes the proportion of the landscape covered by UGS patches, representing the overall extent or percentage of UGS within the study area. The Fragstats 4.2 user manual provides comprehensive information on the specific definitions and calculation formulas of the variables used in the analysis (McGarigal et al., 2012).

In addition to the UGS variables, the water proportion variable (Water) was also calculated using Fragstats 4.2 based on fine-scale data extracted from Tianditu Map. The urban form variables, which reflect traffic volumes and density of urban activities, are represented by road density, 2D and 3D building form variables in this study. Each grid's road density (den_road) represents the total length of main roads per grid area, the 2D building form variable (den_build) refers to the sum of building footprint area per grid area, and the 3D form variable (FAR) is calculated as the product of building footprints and floors, divided by the grid area. The statistical properties for each of these variables are shown in Table 1.

3.3. Spatial statistical methods

This study compared and explored three state-of-art methods: Spatial Lag Model (SLM), which considers spatial diffusion or spillover effect, Multi-scale Geographically Weighted Regression Model (MGWR), which considers spatial heterogeneity and an explanatory machine learning model SHapley Additive exPlanations for eXtreme Gradient Boosting (SHAP for XGBoost) which has the best fitting performance and ability to explain spatial effects. The study implemented SLM, MGWR, and SHAP for XGBoost models using Python's Pysal, spreg, mgwr.gwr, sklearn and SHAP libraries. To validate the accuracy of the models and

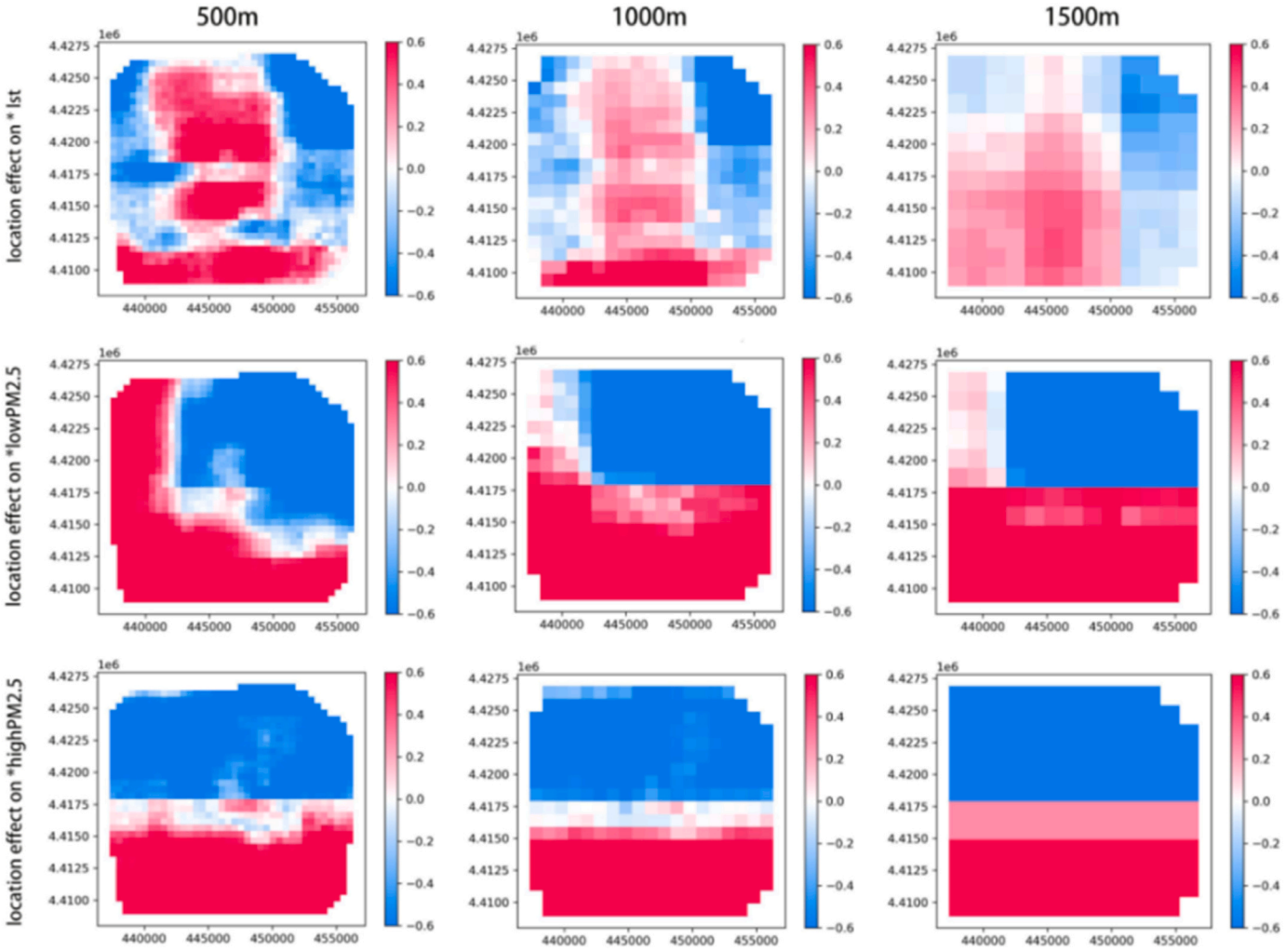

Fig. 3. The location effect on high $PM_{2.5}$, low $PM_{2.5}$ and LSTs indicated by the SHAP values of geographic coordinates. The x and y axes represent longitude and latitude respectively.

Table 2
Comparison of the accuracy of regression models.

		R^2			RMSE			Variance		
		SLM	MGWR	XGBoost	SLM	MGWR	XGBoost	SLM	MGWR	XGBoost
500 m	High $PM_{2.5}$	0.94	**0.97**	0.96	1.00	0.87	**0.19**	0.21	0.22	**0.04**
	Low $PM_{2.5}$	0.98	0.98	**0.98**	1.07	1.04	**0.15**	0.05	0.18	**0.02**
	LSTs	0.91	0.95	**0.96**	0.75	0.62	**0.16**	0.16	0.22	**0.02**
1000 m	High $PM_{2.5}$	0.87	0.90	**0.93**	1.03	0.90	**0.26**	3.90	0.33	**0.07**
	Low $PM_{2.5}$	0.91	0.94	**0.95**	1.48	1.22	**0.29**	3.62	0.38	**0.08**
	LSTs	0.77	0.83	**0.89**	0.83	0.56	**0.27**	3.52	0.38	**0.07**
1500 m	High $PM_{2.5}$	0.75	**0.83**	0.72	0.99	0.81	**0.48**	29.01	0.42	**0.23**
	Low $PM_{2.5}$	0.86	0.90	**0.96**	1.38	1.14	**0.25**	31.01	0.49	**0.06**
	LSTs	0.77	**0.80**	0.63	0.65	0.44	**0.42**	16.11	0.35	**0.18**

the scale effect of the variables, a comparative experiment was conducted on spatial models and machine learning models of different scales of 500 m, 1000 m, and 1500 m, further revealing the potential of machine learning models in spatial research.

SLM is predominantly utilized to investigate the presence of spatial diffusion or spillover effects of the variables (Song et al., 2014; Anselin and Rey, 1991). The equation is as follows:

$$y = \rho W_y + X\beta + \varepsilon \tag{1}$$

This equation involves several variables: y represents the dependent variable, while X is the explanatory variable matrix that lacks an intercept term. β denotes the slope vector, which describes how the explanatory variables influence the output. The spatial weight matrix, W_y, is generated using the Queen matrix, where a value of 1 is assigned to neighboring regions that share a boundary or node, and 0 otherwise. The error term vector is denoted by ε. If the spatial autoregressive coefficient ρ is statistically significant, it suggests a significant spatial correlation among the independent variables, with the value of ρ reflecting the extent of interdependence among individual units, which may be indicative of spatial diffusion or spillover effects.

As an optimization model of geographically weighted regression (GWR), MGWR allows each independent variable to have a different level of spatial smoothness (bandwidth), which is closer to the real spatial model, and has a good explanatory degree and credibility for studying the spatial differentiation characteristics. The formula is as follows. Assuming that there are n grids, for grid $i \in \{1, 2, \ldots, n\}$,

$$y_i = \beta_0 + \sum j \quad \beta_j x_{ij} + \varepsilon_i \tag{2}$$

Where y_i denotes the dependent variable, while x_{ij} is the j_{th} explanatory feature. β_0 is the intercept, while β_j represents the bandwidth used by the coefficient of regression pertaining to the j_{th} feature. The bandwidth of each explanatory variable obtained by adaptive method can reflect the spatial action scale of their respective spatial processes and ε_i denotes the error term vector.

The machine learning model employed in this study utilizes the SHAP-enabled XGBoost model (Li, 2022). The fundamental concept of the SHAP model involves determining the impact that every feature has on the output of the model, and subsequently, to offer both global and local explanations of the "black box" model. The SHAP approach establishes an additive explanatory model that considers all features as "contributors". For every predicted instance, the model generates a forecast, and each feature's SHAP value represents its significance for that sample. To avoid overfitting, the dataset was split into 80 % and 20 %, which were used as the training and test sets respectively. A 5-fold cross-validation approach was employed, where Hyperopt was nested to optimize the hyperparameters. To demonstrate its spatial influence, the SHAP package in Python was utilized for the calculation of the SHAP value. This study used the tree-based SHAP estimation method, which is faster than the kernel-based method and can present different spatial interaction effects. The formula is as follows:

$$f(z') = \varnothing_0 + \sum \varnothing_j z'_j \tag{3}$$

Where f is the explanation model XGBoost, z' is the coalition vector of jth feature. $\varnothing_j$ is the Shapley values of feature j.

To vividly demonstrate the influence of individual features on model predictions, we adopted the dependence plot mode. At the same time, the uncertainty of SHAP estimation is expressed by the light blue shade. The non-parametric bootstrap technique, which involved resampling model residuals and integrating them into prediction outcomes to generate a fresh dependent variable, was employed. Then XGBoost model was retrained with the same hyperparameters, and recalculated and stored the SHAP values. The process was repeated for 5000 times, and bootstrap percentile was used to calculate the 95 % confidence interval of the SHAP value sampling distribution.

4. Results

The estimation results of three dependent variables (high $PM_{2.5}$, low $PM_{2.5}$ and LSTs) and ten independent variables (UGS spatial configuration variables, water proportion, and urban form variables) at three scales are shown in Supplementary Materials Fig. S1.

4.1. Spatial heterogeneity of LSTs and $PM_{2.5}$ concentrations

According to the SHAP values of geographic coordinates, there are distinct spatial patterns in the contribution of different locations to high $PM_{2.5}$, low $PM_{2.5}$ and LSTs, which can be referred as the spatial heterogeneity of $PM_{2.5}$ and LSTs (Fig. 3). It is worth noting that compared to previous methods used to measure spatial heterogeneity, such as GWR, these spatial heterogeneity patterns have considered other independent factors and exclusively reflect the contributions of geographical locations. Positive location contributions are indicated by the red areas, whereas the blue areas correspond to places with negative location contributions.

At the scale of 500 m, the spatial heterogeneity of the three dependent variables is most pronounced. The high and low $PM_{2.5}$ show obvious north-south regional distribution differences, particularly for high $PM_{2.5}$, which are mainly due to regional transmission being the main source of high air pollution in Beijing. In terms of LSTs, a pattern of elevated values in the central and southern regions, and decreased values in the peripheral and northern regions, can be observed, indicating a clear central-peripheral distribution pattern. This pattern is primarily due to the central-peripheral development mode in Beijing, where there is a high density in the center and relatively low density in the periphery.

4.2. Spatial regression results for LSTs and $PM_{2.5}$ concentration

For all dependent variables at all scales, with the exception of high $PM_{2.5}$ at 500 m and 1500 m scales, and LSTs at 1500 m scale, the R^2 values of machine learning methods were the highest, and the RMSE and

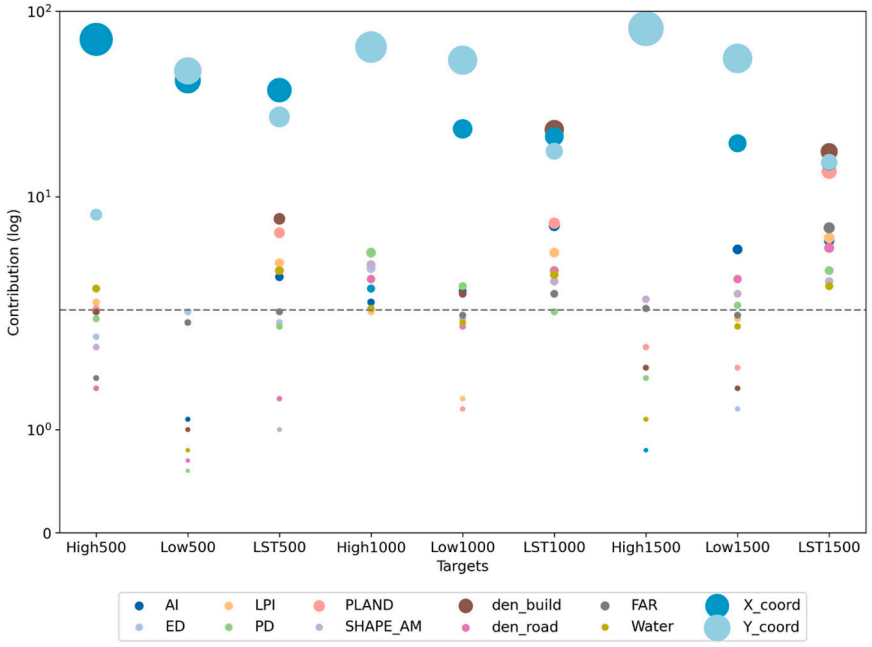

Fig. 4. Contribution rates of independent variables.

Table 3
Contribution rates of all variables (%).

	500 m			1000 m			1500 m		
	High $PM_{2.5}$	Low $PM_{2.5}$	LSTs	High $PM_{2.5}$	Low $PM_{2.5}$	LSTs	High $PM_{2.5}$	Low $PM_{2.5}$	LSTs
AI	1.8	1.1	**3.7**	**2.7**	**3.1**	**7**	1.8	**5.2**	**5.8**
ED	1.9	2.4	2.1	**4.1**	2	2.4	1.6	1.2	**3.3**
LPI	**2.7**	1	**4.4**	2.4	1.3	**5**	1.8	2.2	**6**
PD	2.2	0.6	2	**5**	**3.3**	2.4	1.5	**2.6**	**4**
PLAND	**2.5**	0.7	**6.4**	**2.5**	1.2	**7.2**	1.8	1.6	**13.7**
SHAPE_AM	1.8	0.7	1	**4.3**	2.2	**3.5**	**2.8**	**3**	**3.5**
den_build	2.4	1	**7.6**	**3.2**	**3**	**23**	1.6	1.4	**17.5**
den_road	1.4	0.7	1.3	**3.6**	2	**4**	**2.5**	**3.6**	**5.3**
FAR	1.5	2.1	2.4	**2.5**	2.3	**3**	**2.5**	2.3	**6.8**
Water	**3.2**	0.8	**4**	**2.5**	2.1	**3.8**	1.1	2	**3.3**
X_coord	8	42.3	37.5	3.2	23.2	21.1	0.8	19.4	15.3
Y_coord	70.4	47.6	26.9	64	54.4	17.6	80.6	55.6	15.4

Note: The bolded values represent the contribution rates that are among the top 50 %.

variance values of machine learning methods were the lowest (Table 2). Notably, the analysis reveals that the variance is lower when working with smaller-scale data. For instance, the lowest variance is observed at the 500-meter scale. Overall, the comparison results indicated that the machine learning regression models achieved a better fitting effect than traditional spatial statistical models. Additionally, the coefficients of the SLM and MGWR models are listed in Appendix Tables S1 and S2, respectively.

As shown in Fig. 4 and Table 3, location variables were the largest contributors for almost all dependent variables and all scales. Therefore, this study focus on the top 50 % ranks of contributions among non-location variables, i.e., variables with a contribution rate above 2.45 % as shown by the dashed line in Fig. 4. The contribution of variables affecting high $PM_{2.5}$ varies little at the 500- and 1500-meter scales, but increases sharply at the 1000-meter scale. The contribution rates of variables affecting low $PM_{2.5}$ gradually increased from 500 m to 1500 m scale, reaching 25.1 % at 1500 m. This may be due to local emissions, such as vehicle exhaust, in addition to regional transmissions, contributing to low $PM_{2.5}$. For LSTs, the contribution of all non-location variables gradually increased from 34.9 % at the 500 m scale to 69.2 % at the 1500 m scale. This is because the primary source of LSTs is solar radiation, and there is less neighborhood heat exchange transmission than that of $PM_{2.5}$.

At the 500 m scale, for high $PM_{2.5}$, both the UGS proportion and the largest patch proportion were equally important (2.5 % and 2.7 %, respectively), and water proportion could also influence high $PM_{2.5}$ (3.2 %). For low $PM_{2.5}$, no variables were included in top 50 % of the contribution rate ranking. For LSTs, the contribution of UGS proportion (6.4 %) was higher than that of any UGS morphology variable, but lower than the total contribution of UGS morphology (8.1 %). Building density had the greatest influence on LSTs (7.6 %), followed by the proportion of the largest UGS patch (4.4 %) and the aggregated distribution of UGS patches (3.7 %). Water proportions also had an influence on LSTs (4.0 %).

At the 1000 m scale, the contribution of UGS proportions remained unchanged for high $PM_{2.5}$ (2.5 %). However, the contributions of several UGS morphology variables, especially UGS patch density, have increased. Density of buildings and roads, and water proportions could also influence high $PM_{2.5}$. For low $PM_{2.5}$, UGS proportions became less important and UGS aggregation and patch density had the greatest contributions (3.1 % and 3.3 %, respectively). For LSTs, the total contribution of UGS morphology variables (15.5 %) was much higher than that of UGS proportion (7.2 %). Similar to the 500 m scale, AI and LPI were the two UGS morphology variables with the highest

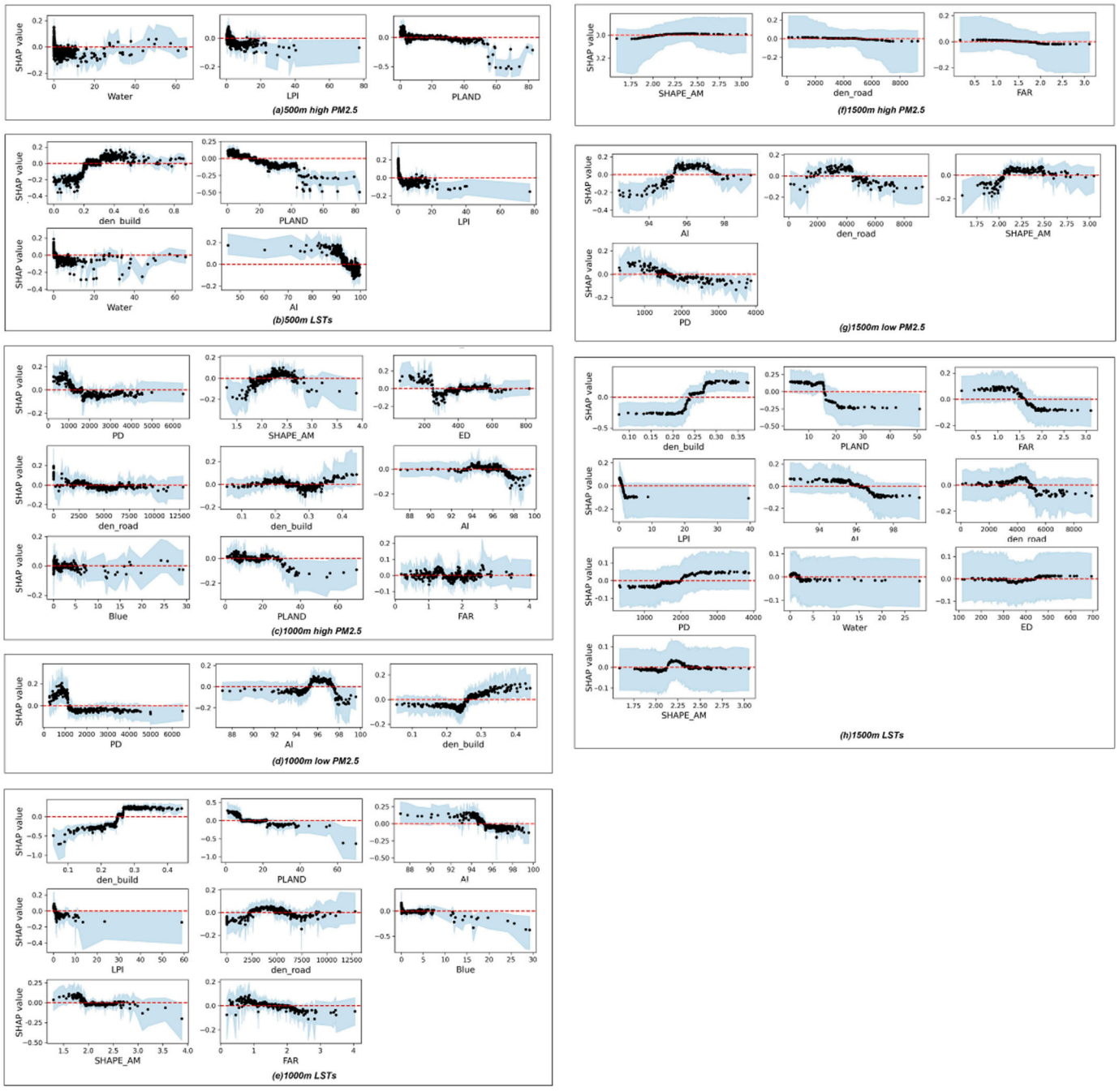

Fig. 5. Partial dependence plots for the non-location features with a contribution rate ranking in the top 50 % (exceeding 2.45 %). The blue shaded region indicates the 95 % confidence interval of SHAP values obtained from bootstrapping.

contributions.

At the 1500 m scale, non-location variables had the lowest contribution to high $PM_{2.5}$ among the three scales. The number of variables influencing low $PM_{2.5}$ reached a maximum, and UGS proportion was still not included. All variables had a contribution ranking in the top 50 % for LSTs. Building density had the greatest impact (17.5 %). The contribution of UGS proportion increased (13.7 %), while the contribution of UGS morphology reached its maximum (22.6 %), with the largest UGS patch proportion being the most important UGS morphology variable (6 %).

4.3. Confidence intervals for SHAP values

Partial dependence plots for features other than location (extended version) were shown in Supplementary Material Fig. S2. SHAP partial dependence plots typically have the feature of interest plotted on the x-axis, representing its varying values. The y-axis, on the other hand, represents the SHAP values. These values indicate the contribution of that feature to each individual prediction, allowing us to see the direction and magnitude of the feature's impact on the model's predictions. The non-location features that ranked within the top 50 % of contributions, meaning those with a contribution rate exceeding 2.45 %, were shown in Fig. 5. Accordingly, the contributions of all non-location variables to the dependents at the grid scale, measured by SHAP values of geographic coordinates, were shown in Supplementary Material Fig. S3.

At the 500 m scale, for high $PM_{2.5}$, LPI was strongly positively correlated with $PM_{2.5}$ between 0.00 % and 2.00 %, and negatively correlated between 2.00 %–4.85 %, and no influence afterwards. There

was a strong decrease before 4.00 % for PLAND, and was negatively correlated between 4.00 %–30.00 %, the correlation was weak afterwards since the wide confidence interval. Water proportions was strongly negatively correlated before 1.50 %, and no influence afterwards. For LSTs, UGS proportions was strongly negative correlated before 25.00 % and remained stable until 42.00 %. After 42.00 %, the correlation seemed to be enhanced but its weak due to the wide confidential intervals. The aggregated distribution (AI) of UGS was strongly negatively correlated at the value of 92.50–97.50, and no influence after. The largest proportion of UGS patch was strongly negatively correlated before 7.00 %. Building density was strongly positively correlated before 35 %, and the relationship remains stable afterwards. Water proportion was also strongly negatively correlated before 7.50 %, and no effect afterwards.

At the 1000 m scale, for high $PM_{2.5}$, ED and SHAPE_AM were both positively correlated with $PM_{2.5}$, between the value of 320.00–560.00 and 1.75–2.55, respectively. Both PD and AI exhibited a negative correlation with $PM_{2.5}$, between the value of 800.00–1650.00 and 96.00–97.85, respectively. UGS proportions was weakly negatively correlated between the value of 25.00–30.00 %. No clear relationship between building density, FAR and road density with high value $PM_{2.5}$. For low $PM_{2.5}$, PD was negatively correlated between the value of 880.00–1500.00 and remained stable afterwards. The aggregated distribution of UGS was positively correlated with low $PM_{2.5}$ between 94.50 and 95.80, and negatively correlated from 97.00 to 98.00. No clear relationship was for building density. In terms of LSTs, UGS proportions was negatively correlated before 22.00 %, the negative correlation enhanced between 22.00 % and 38.00 %, and no clear relationship afterwards. Aggregated UGS distribution was negatively correlated from 94.00 to 95.55, and the influence remained stable afterwards. LPI was strongly negatively correlated from 0.00 % to 2.50 %, and the influence remained stable afterwards, while the relationship was weak. Shape complexity (SHAPE_AM) was negatively correlated from 1.75 to 1.95, the influence remained stable from 2.0 to 2.5, and no influence afterwards. Density of roads was positively correlated from 1900.00 to 3300.00, and negatively correlated from 4750.00 to 7650.00. Water proportions was negatively correlated before 1.00 %, and the relationship remained stable to 5.00 %. FAR was negatively correlated between 1.18 and 2.35, and building density was positively correlated between 17 %–0.26 %, and the relationship remained stable afterwards.

At the 1500 m scale, most relationships were weak as all the confidence intervals were wide, which caused by the large reduction of the samples. For low $PM_{2.5}$, aggregated UGS distribution was positively correlated from 94.50 to 95.80, and negatively correlated from 97.00 to 97.80. Shape complexity was positively correlated from 1.90 to 2.15, the relationship remained stable to 2.50, and no influence afterwards. Densities of UGS patch and road were negatively correlated between 1150.00 and 2750.00, and 4200.00–6500.00.

5. Discussion

In highly-dense urban areas, reorganizing small-scale UGS patches and optimizing their spatial configurations is a proper option to achieve greater ecological benefits. However, limited studies have investigated their mitigation effects on $PM_{2.5}$ concentrations and LSTs simultaneously. The objective of this study is to investigate the optimal spatial arrangement of UGS with a constrained proportion. Additionally, urban morphological variables that affect air quality and urban thermal environment are also considered as contributing factors, which allows for a more comprehensive investigation of urban sustainability and ecological benefits. Most importantly, an explanatory machine learning method was employed to reveal the nonlinear relationships among variables in the spatial context.

5.1. The advantages of using explanatory machine learning regression model

The use of an explanatory machine learning regression model, which includes the SHAP local interpretation method specifically designed for spatial data, have several advantages compared to traditional spatial regression models. The advantages are primarily reflected in three key aspects. Firstly, it improved accuracy. Machine learning methods can identify complex patterns and relationships that traditional statistical models may not be able to capture. The results suggested that the machine learning models had higher R^2 values and lower RMSE values than traditional statistical models, especially for $PM_{2.5}$, indicating a better fit to the spatial data. Secondly, it provides spatially explicit information. SHAP for machine learning methods can provide spatially explicit information about the contribution of locations to the dependent variables, as demonstrated by the clear spatial patterns of SHAP values of geographic coordinates, which have been excluded from the effects of independent variables. This information can help us to better understand the spread and location of these environmental problems. Thirdly, it improves understanding of complex relationships. Machine learning methods can identify complex relationships between dependent and independent variables, including interactions and nonlinear relationships, thereby determining effective value ranges. This can enhance our understanding of the underlying drivers behind the distribution of pollution and high temperature.

5.2. Co-mitigation effects of UGS variables on $PM_{2.5}$ concentrations and LSTs

Drawing upon the findings from the 500 m, 1000 m, and 1500 m scales, this study concludes that the proportion of UGS should be maintained between 25 % and 30 %, and there is no need to exceed 40 %, which could be appropriate for mitigating high $PM_{2.5}$ and LSTs, and more determinant for the latter. Previous studies have confirmed that a higher UGS proportion could reduce the PM2.5 values' daily average, minimum, and maximum (Chen et al., 2019). Increasing UGS proportion is more effective in mitigating urban microclimates than other approaches, with Yuan et al. claiming that a UGS proportion of 20 % has a greater potential for improving urban microclimate (Yuan et al., 2017), which is similar with the findings of this study.

For UGS landscape metrics, there is mitigation effects for all three issues when the aggregation index of UGS was above 97, indicating a high level of aggregated condition and suggesting that more aggregated UGS patches could be of better mitigation roles. This finding aligns with earlier research, which indicated that UGS can remove $PM_{2.5}$ more effectively when UGS patches are situated in closer proximity and are more contiguous with one another (Li et al., 2023).

Most previous studies identified larger UGS largest patches as having better mitigation effects (Bagheri et al., 2017). This study found that the largest UGS patch proportion between 2.00 % and 4.85 % could achieve mitigation effects for all three issues. The proportion was not very high, indicating that higher proportions are not necessarily better. A UGS patch density of above 1650 could mitigate all three issues, which is not a very high level of patch density, while most previous studies suggested that higher patch densities have an intensifying effect (Yu et al., 2020). There is a conflict in terms of shape complexity, as higher shape complexity serves an intensifying role for $PM_{2.5}$, but a mitigation role for LSTs. This is different from some previous studies (Bi et al., 2022a; Łowicki, 2019), which suggest that elevated shape complexity could improve adhesion capacity of UGS patches to $PM_{2.5}$ by enhancing their contact with other land types (Xu et al., 2021). However, patches that are larger in size with intricate shapes or exceed a specific PLAND threshold may result in the configuration having a more significant impact (Masoudi and Tan, 2019). For edge density, there is no value for co-mitigation.

Fig. 6. Samples of green spaces within effective indicator thresholds. Red color indicates exceeding the thresholds.

5.3. Co-mitigation effects of non-UGS variables on $PM_{2.5}$ concentrations and LSTs

The urban pattern is shaped by the urban form and the UGS pattern, and both variables can have an impact on the urban thermal environment and air pollution. The proportion of water bodies at 1.5 % has been identified to have a mitigation effect on high $PM_{2.5}$ and LSTs, and maintaining a higher proportion is not necessary. However, previous studies (Steeneveld et al., 2014; Hathway and Sharples, 2012) suggested a negative correlation between water proportion and these two environmental issues. Surprisingly, a higher road density appears to mitigate both $PM_{2.5}$ and LSTs, despite the fact that it usually indicates higher traffic-related heat and air pollution emissions. This may be due to a decrease in overall road density in areas with higher main road density, as the study only focused on main roads in the city. Building density and FAR do not appear to have any co-mitigation value, but they have a significant impact on LSTs.

5.4. Strengthens and limitations

The strengths of this study are as follows. The co-mitigation effects of UGS morphology on winter $PM_{2.5}$ and summer LSTs were investigated, as effectively allocating limited UGS in highly-dense urban areas is a challenge. A new UGS data source that depicted vegetated land with consistent boundaries for each season was introduced, providing more advantageous results from an engineering perspective. An explanatory machine learning regression method was employed, which is a good alternative to traditional spatial statistical models and can estimate accurate spatial effects and non-linear relationships.

However, this study also has limitations. Firstly, our analysis may not have fully accounted for large-scale spatial trends, such as the spatial distribution of fine particles across entire cities, which could potentially impact the results of the statistical analysis regarding UGS mitigation effects. The study predominantly concentrated on smaller spatial patterns quantified through landscape metrics, without an exhaustive exploration of potential influences at higher spatial scales. Secondly, the influence of the surrounding built-up areas was not taken into consideration. Moreover, due to data limitations, we were only able to examine mitigation effects within a single time period. In the absence of specific traffic flow data, road density was employed as a proxy to represent traffic flow. Additionally, the study also failed to consider the spatial distribution of various vegetation types in Beijing, which hindered the comparison of mitigation effects among different plant species. Notably, Platycladus orientalis and Pinus tabulaeformis, two evergreen species prevalent in Beijing, exhibit high potential for fine particle removal (Wang et al., 2022).

In the future, causal analysis methods such as Granger causality test, combined with machine learning approaches, can be employed to disentangle causes and effects of $PM_{2.5}$ and LST.

6. Conclusion

This study aims to explore the co-mitigation mechanisms of winter $PM_{2.5}$ concentrations and summer LSTs in highly-dense urban areas of Beijing, China. To eliminate scale effects, explanatory variables including UGS spatial configurations, water proportions, and urban morphology, were examined at three scales of 500 m, 1000 m, and 1500 m. Explanatory machine learning methods were used to analyze the spatial data. The main findings are summarized below.

Maintaining UGS proportions between 25 % and 30 % is appropriate for mitigating high $PM_{2.5}$ and LSTs, with a greater impact on LSTs. UGS proportion exceeding 40 % does not significantly improve the mitigation effect. UGS morphology plays a more significant role in mitigating $PM_{2.5}$ concentrations than LSTs. Higher UGS aggregation (above 97) and UGS patch density (above 1650) were capable of mitigating both $PM_{2.5}$ concentrations and LSTs. The proper proportion of the largest UGS patch (2.00–4.85 %) also have similar mitigation effects. However, UGS patches with higher shape complexity intensifies $PM_{2.5}$ concentrations but mitigates LSTs, leading to a conflicting role. The sample images showcasing effective mitigation strategies within the threshold are presented in Fig. 6. These visual references are intended to provide practical insights and guidance for urban planners and designers.

Additionally, maintaining a proportion of water bodies at 1.5 % has a mitigation effect on high $PM_{2.5}$ and LSTs, and maintaining a higher proportion is unnecessary. Surprisingly, a higher density of main roads (above 4750) appears to mitigate both $PM_{2.5}$ and LSTs. This may be because in areas with higher main road density, overall road density decreases, as the study only focuses on main roads rather than all roads in the city.

CRediT authorship contribution statement

Yan Li: Conceptualization, Methodology, Writing – original draft preparation and Writing – Reviewing and Editing. **Yecheng Zhang**: Methodology, Visualization and Writing – Reviewing and Editing. **Qilin Wu**: Funding and Writing – Reviewing and Editing. **Ran Xue**: Visualization. **Xiaoran Wang:** Visualization. **Menglin Si**: Data curation, Writing – Reviewing and Editing. **Yuyang Zhang**: Conceptualization, Data curation, Funding, Methodology, Supervision, Visualization, Writing – original draft preparation and Writing – Reviewing and Editing.

Declaration of Competing Interest

The authors declare that they have no known competing financial interests or personal relationships that could have appeared to influence the work reported in this paper.

Acknowledgements

This research was supported by grant from the China Postdoctoral Science Foundation [2019TQ0166]. The authors would like to thank Wenke Ma, Ke Gao, Pengcheng Du, Yuhan Li, and Xiaoya Fang from YNY Lab, North China University of Technology for supporting the research. In addition, all authors declare no conflicts of interest.

Appendix A. Supporting information

Supplementary materials associated with this article can be found in the online version at doi:10.1016/j.ufug.2023.128086.

References

Ali-Toudert, F., Mayer, H., 2007. Effects of asymmetry, galleries, overhanging facades and vegetation on thermal comfort in urban street canyons. Sol. Energy 81 (6), 742–754.
Anselin, L., Rey, S., 1991. Properties of tests for spatial dependence in linear regression models. Geogr. Anal. 23 (2), 112–131.
Bagheri, Z., Nadoushan, M.A., Abari, M.F., 2017. Evaluation of the effect of green space on air pollution dispersion using satellite images and landscape metric: a case study of Isfahan City. Fresenius Environ. Bull. 26 (12A), 8135–8145.
Beckett, K.P., Freer-Smith, P., Taylor, G., 2000. Particulate pollution capture by urban trees: effect of species and windspeed. Glob. Change Biol. 6 (8), 995–1003.
Bi, S., et al., 2022a. A new framework for analysis of the morphological spatial patterns of urban green space to reduce PM2. 5 pollution: a case study in Wuhan, China. Sustain. Cities Soc., 103900
Bi, S., et al., 2022b. A new framework for analysis of the morphological spatial patterns of urban green space to reduce PM2. 5 pollution: A case study in Wuhan, China, 82. Sustainable Cities and Society.
Chan, E.Y.Y., et al., 2012. A study of intracity variation of temperature-related mortality and socioeconomic status among the Chinese population in Hong Kong. J. Epidemiol. Community Health 66 (4), 322–327.
Chen, A., et al., 2014. How many metrics are required to identify the effects of the landscape pattern on land surface temperature? Ecol. Indic. 45, 424–433.
Chen, M., et al., 2019. Effects of neighborhood green space on PM2. 5 mitigation: evidence from five megacities in China. Build. Environ. 156, 33–45.
Chestnut, L.G., et al., 1998. Analysis of differences in hot-weather-related mortality across 44 US metropolitan areas. Environ. Sci. Policy 1 (1), 59–70.
Connors, J.P., Galletti, C.S., Chow, W.T., 2013. Landscape configuration and urban heat island effects: assessing the relationship between landscape characteristics and land surface temperature in Phoenix, Arizona. Landsc. Ecol. 28 (2), 271–283.
EPA, U., 2012. Revised Air Quality Standards For Particle Pollution And Updates To The Air Quality Index (AQI). US EPA,.
Han, L., Zhou, W., Li, W., 2015. City as a major source area of fine particulate (PM2. 5) in China. Environ. Pollut. 206, 183–187.
Hathway, E., Sharples, S., 2012. The interaction of rivers and urban form in mitigating the Urban Heat Island effect: a UK case study. Build. Environ. 58, 14–22.
Huang, C., et al., 2017. Green spaces as an indicator of urban health: evaluating its changes in 28 mega-cities. Remote Sens. 9 (12), 1266.
Huang, Q., Lu, Y., 2018. Long-term trend of urban heat island intensity and climatological affecting mechanism in Bejing city. Sci. Geogr. Sin. 38 (10), 1715–1723.
Imhoff, M.L., et al., 2010. Remote sensing of the urban heat island effect across biomes in the continental USA. Remote Sens. Environ. 114 (3), 504–513.
Khan, F.I., Abbasi, S., 2001. Effective design of greenbelts using mathematical models. J. Hazard. Mater. 81 (1–2), 33–65.
Kim, K.-H., Kabir, E., Kabir, S., 2015. A review on the human health impact of airborne particulate matter. Environ. Int. 74, 136–143.
Li, K., et al., 2023. Quantitative estimation of the PM2. 5 removal capacity and influencing factors of urban green infrastructure. Sci. Total Environ., 161476
Li, Z., 2022. Extracting spatial effects from machine learning model using local interpretation method: an example of SHAP and XGBoost. Comput., Environ. Urban Syst. 96, 101845.
Lin, T.-P., Matzarakis, A., Hwang, R.-L., 2010. Shading effect on long-term outdoor thermal comfort. Build. Environ. 45 (1), 213–221.
Lin, Y., et al., 2020. Water as an urban heat sink: blue infrastructure alleviates urban heat island effect in mega-city agglomeration. J. Clean. Prod. 262, 121411.
Lo, A.Y., Jim, C.Y., 2012. Citizen attitude and expectation towards greenspace provision in compact urban milieu. Land Use Policy 29 (3), 577–586.
Łowicki, D., 2019. Landscape pattern as an indicator of urban air pollution of particulate matter in Poland. Ecol. Indic. 97, 17–24.
Masoudi, M., Tan, P.Y., 2019. Multi-year comparison of the effects of spatial pattern of urban green spaces on urban land surface temperature. Landsc. Urban Plan. 184, 44–58.
McDonald, A., et al., 2007. Quantifying the effect of urban tree planting on concentrations and depositions of PM10 in two UK conurbations. Atmos. Environ. 41 (38), 8455–8467.
McGarigal, K., S.A. Cushman, and E. Ene, *FRAGSTATS v4: spatial pattern analysis program for categorical and continuous maps*. Computer software program produced by the authors at the University of Massachusetts, Amherst. ⟨http://www.umass.edu/landeco/research/fragstats/fragstats.html⟩, 2012. **15**.
Organization, W.H., 2006. Air quality guidelines: global update 2005: particulate matter, ozone, nitrogen dioxide, and sulfur dioxide. World Health Organization,.
Peng, J., et al., 2016. Urban thermal environment dynamics and associated landscape pattern factors: a case study in the Beijing metropolitan region. Remote Sens. Environ. 173, 145–155.
Peng, J., et al., 2018. Seasonal contrast of the dominant factors for spatial distribution of land surface temperature in urban areas. Remote Sens. Environ. 215, 255–267.
Si, M., et al., 2022. Spatiotemporal pattern and long-term trend of global surface urban heat islands characterized by dynamic urban-extent method and MODIS data. ISPRS J. Photogramm. Remote Sens. 183, 321–335.
Song, J., et al., 2014. The relationships between landscape compositions and land surface temperature: quantifying their resolution sensitivity with spatial regression models. Landsc. Urban Plan. 123, 145–157.
Steeneveld, G.J., et al., 2014. Refreshing the role of open water surfaces on mitigating the maximum urban heat island effect. Landsc. Urban Plan. 121, 92–96.

Wan, Z., 2014. New refinements and validation of the collection-6 MODIS land-surface temperature/emissivity product. Remote Sens. Environ. 140, 36–45.
Wang, Y., Feng, Z., Ma, W., 2022. Analysis of tree species suitability for plantation forests in Beijing (China) using an optimal random forest algorithm. Forests 13 (6), 820.
Wei, J., et al., 2021. Reconstructing 1-km-resolution high-quality PM2. 5 data records from 2000 to 2018 in China: spatiotemporal variations and policy implications. Remote Sens. Environ. 252, 112136.
Xu, W., et al., 2021. Analysis of spatiotemporal variation of PM2. 5 and its relationship to land use in China. Atmos. Pollut. Res. 12 (9), 101151.
Yang, J., et al., 2017. Assessing the impacts of urbanization-associated green space on urban land surface temperature: A case study of Dalian, China, 22. Urban Forestry & Urban Greening,, pp. 1–10.
Yu, Z., et al., 2020. Critical review on the cooling effect of urban blue-green space: a threshold-size perspective. Urban For. Urban Green. 49, 126630.
Yuan, J., Emura, K., Farnham, C., 2017. Is urban albedo or urban green covering more effective for urban microclimate improvement?: A simulation for Osaka. Sustain. Cities Soc. 32, 78–86.
Zhang, Y., et al., 2021. Measuring community green inequity: a fine-scale assessment of Beijing Urban Area. Land 10 (11), 1197.
Zhao, L., et al., 2021. Effect of urban lake wetlands and neighboring urban greenery on air PM10 and PM2. 5 mitigation. Build. Environ. 206, 108291.
Zhou, W., Wang, J., Cadenasso, M.L., 2017. Effects of the spatial configuration of trees on urban heat mitigation: a comparative study. Remote Sens. Environ. 195, 1–12.
Zhang, Y., et al., 2023. Neighborhood infrastructure-related risk factors and non-communicable diseases: a systematic meta-review. Environ. Health 22 (1), 1–15.
Zhang, Y., et al., 2023. Predicting highly dynamic traffic noise using rotating mobile monitoring and machine learning method. Environ. res. 229, 115896.